Invited Paper

# High contrast imaging with a self-coherent camera

Raphaël Galicher[a,b] Johan Mazoyer[b] Pierre Baudoz[b] Gérard Rousset[a,b]

[a] Université Paris Diderot, 3 rue Thomas Mann, 75013 Paris, France
[b] Lesia, CNRS, Observatoire de Paris, 5, place Jules Janssen, 92195 Meudon, France

## ABSTRACT

Direct imaging of exoplanets is very challenging because the planet is $10^4$ to $10^{10}$ fainter than the star at a separation of a fraction of arcsec. Several coronagraphs have been proposed to reduce the contrast ratio but their performance strongly depends on the level of phase and amplitude aberrations that induce speckles in the science image. An active control of the aberrations and a posteriori calibration are thus required to reach very high contrasts. Classical adaptive optics are not sufficient for this purpose because of non-common path aberrations. Our team proposed a self-coherent camera that spatially modulates the speckles in the science image. It is then possible to both actively control a deformable mirror and calibrate the residuals a posteriori. The current paper is an overview of the developments we have been working on for 7 years. We present the principle of the self-coherent camera, laboratory performance obtained in monochromatic light, and upgrades of the technique to make it achromatic.

**Keywords:** Instrumentation, High contrast imaging, High angular resolution, exoplanet, wavefront correction, dark hole, adaptive optics, differential imaging

## 1. INTRODUCTION

Since the 90s, about 1000 exoplanets have been discovered using indirect techniques as radial velocity and transits. From this sample, several teams derived the planetary frequency as a function of the planetary mass, planet-star separation, star metallicity, and so on. However, because of detection biases, it is well known that the planet sample is not complete for planets that orbit in the outer part of their system (> a few AUs). Today, the only technique that can probe these planets is direct imaging that started to give results in 2009 with the detection of $\beta$-Pictoris b [1] and HR 8799 planets.[2] Direct imaging is also very attractive because it is the only technique that can provide spectroscopic information on these outer planets – transits being used for planets closer than ∼1 AU. But a planet is usually $10^4$ to $10^{10}$ fainter than its star and separated by a fraction of arcsec. Thus, only a dedicated instrument can provide a resolved image of the system.

For imaging in visible light, different coronagraphs have been proposed to modify the distribution of light of the central star in a pupil plane or in a focal plane or in both planes with the same final objective: suppress the stellar light without alterating the planet signal.[3–8] Our team proposed, developed, tested,[9–11] and/or provided coronagraphs for several intruments as MIRI on the JWST,[12] NACO at VLT,[13,14] or SPHERE at VLT. Most of these devices are very efficient if the beam is not aberrated. However, phase and amplitude aberrations cannot be avoided: atmospheric turbulence, thermal breathing of optics, flexures of mounts, phase and amplitude aberrations on optical surfaces, etc. It is thus required to correct for these aberrations to make the coronagraphs work in optimized conditions and reach high contrast images.

Classical adaptive optics systems are very useful to minimize the impact of the atmospheric turbulence. The beam collected by the telescope is usually split into two channels. The science channel where the image of interest is recorded and the wavefront sensing (WFS) channel where the aberrations to be corrected are estimated. Once estimated, a deformable mirror is used to minimize the aberrations in the WFS channel and thus, improve the quality of the image in the science channel. However, the estimated aberrations in the WFS channel differ from the aberrations that exist in the science channel: there are aberrations of the science channel that are not estimated and aberrations in the WFS channel that do not exist in the science channel. The impact of these non-common path aberrations (NCPA) is dramatic for coronagraphy: they let part of the stellar light

E-mail: raphael.galicher@obspm.fr, Phone number: +33 (0)1 45 07 75 83

Techniques and Instrumentation for Detection of Exoplanets VI, edited by Stuart Shaklan, Proc. of SPIE
Vol. 8864, 88640M · © 2013 SPIE · CCC code: 0277-786X/13/$18 · doi: 10.1117/12.2025298

leaking through the instrument and inducing speckles in the science image, which strongly limit the contrast in the image. Moreover, for both a ground-based or a space-based telecope, the NCPA evolve in time (flexures, temperature changes, etc) and a new stage in the instrument is required to estimated for them directly from the science image.

Differential imaging techniques do the estimation a posteriori modulating the speckles intensity with respect to the planet signal using, for example, angular rotation of the field-of-view,[15] spectral signatures,[16] or light polarization differences.[17] They are very useful to enhance the contrast of the raw images by a factor of 10 or 100. The performance in the final image is thus directly linked to the contrast in the raw images. And the only way to improve the raw image quality is the active correction of the aberrations using the science image to remain NCPA-free. Several concepts exist for this wavefront sensing in focal plane. Most of them use a temporal modulation of the speckles to retrieve the complex amplitude of their electric field.[18–20] Our team proposed a self-coherent camera (SCC) that uses spatial modulation instead.[21,22]

In this paper, we briefly recall the principle of the SCC and we explain how we use it to control a deformable mirror to create a dark hole in the science image (§ 2). In § 3, we give the status of the high contrast imaging bench called THD-bench that we developed to test different coronagraphs, focal plane wavefront sensors, and differential imaging techniques under the same conditions. Then, we report experimental performance of the SCC in monochromatic light. Finally, we discuss the possible upgrades of the SCC to make it achromatic in § 4.

## 2. PRINCIPLE OF THE SCC

The self-coherent camera (SCC) has already been presented in several papers.[21–31] Here, we briefly recall the principle of the technique (§ 2.1) and how we use the spatial modulation of the speckles (§ 2.2) to control a deformable mirror and create a dark hole in the science image (§ 2.3). We encourage the reader to refer to the previous papers for exhaustive parametric studies of the instrument configuration.

### 2.1 Spatial modulation of speckles

Fig. 1 presents a scheme of the association of a self-coherent camera with a focal plane phase mask coronagraph. The beam incoming from the telescope hits a deformable mirror and converges on the focal plane mask of the

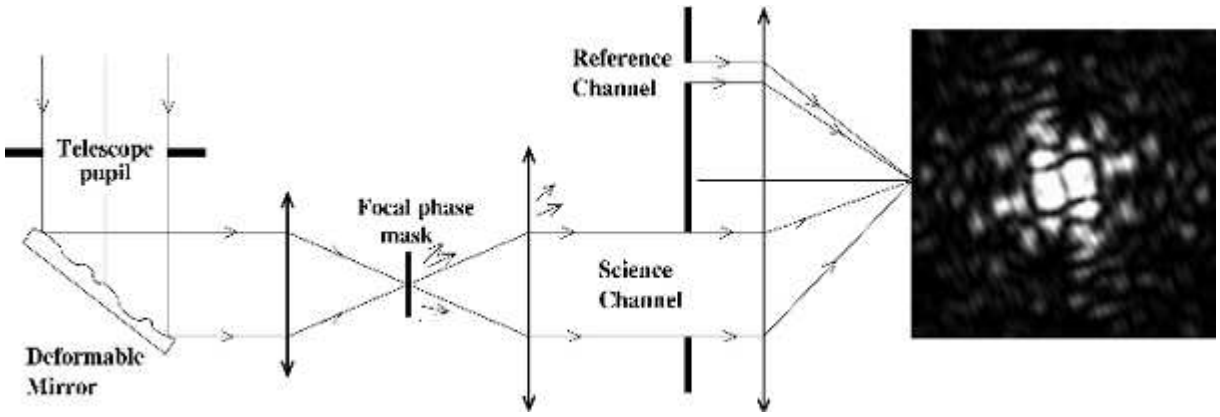


Figure 1. *Association of a self-coherent camera and a coronagraph.*

coronagraph. The mask scatters the light of the on-axis source, the star, outside the geometrical pupil in the following pupil plane. There, a small reference hole is added to the classical Lyot stop to add a reference channel to the science channel. We recall that the light of any off-axis source (planet for example) as well as the light that induces the stellar speckles in the science image because of aberrations are not affected by the focal plane mask and thus, go through the science channel. The reference channel contains only part of the light that is scattered by the focal plane mask. The last optics make the two channels interfer in a Fizeau pattern in the science image.

In this image, the stellar speckles are spatially modulated by the Fizeau fringes whereas the planet image is not modulated as its light is not coherent with the stellar light that goes through the reference channel.

All these remarks come from the interpretation of the mathematical expression of the intensity in the science image that we derived in a previous work[27]

$$I(\alpha) = \int_{\mathcal{R}} \frac{1}{\lambda^2} \Big[ I_{\rm S}\left(\frac{\alpha D}{\lambda}\right) + I_{\rm R}\left(\frac{\alpha D}{\lambda}\right) + I_{\rm C}\left(\frac{\alpha D}{\lambda}\right) \\ +2Re\left( A_{\rm S}\left(\frac{\alpha D}{\lambda}\right) A^*_{\rm R}\left(\frac{\alpha D}{\lambda}\right) \exp\left(\frac{2i\pi\alpha\xi_0}{\lambda}\right)\right)\Big] d\lambda, \quad (1)$$

where $\alpha$ is the angular coordinate in the science image, $\lambda$ is the wavelength, $D$ is the Lyot stop diameter, $\xi_0$ is the center-to-center separation in the Lyot plane between the reference and the science channel. $A_S$ ($I_S = |A_S|^2$) and $A_R$ ($I_R = |A_R|^2$) are the focal plane complex electric field (intensities) associated to the speckles and to the reference channel respectively. $I_C$ is the planet intensity. The wavelength bandpass is $\mathcal{R} = [\lambda_0 - \Delta\lambda/2, \lambda_0 + \Delta\lambda/2]$.

## 2.2 Speckle complex electric field

Taking the Fourier transform of $I$ (Eq. 1), we obtain three well-separated peaks (Fig. 2) if $\xi_0 > 1.5D$ (we discuss this assumption in § 4.2). The central peak is the sum of the autocorrelations of the speckle intensity, of the

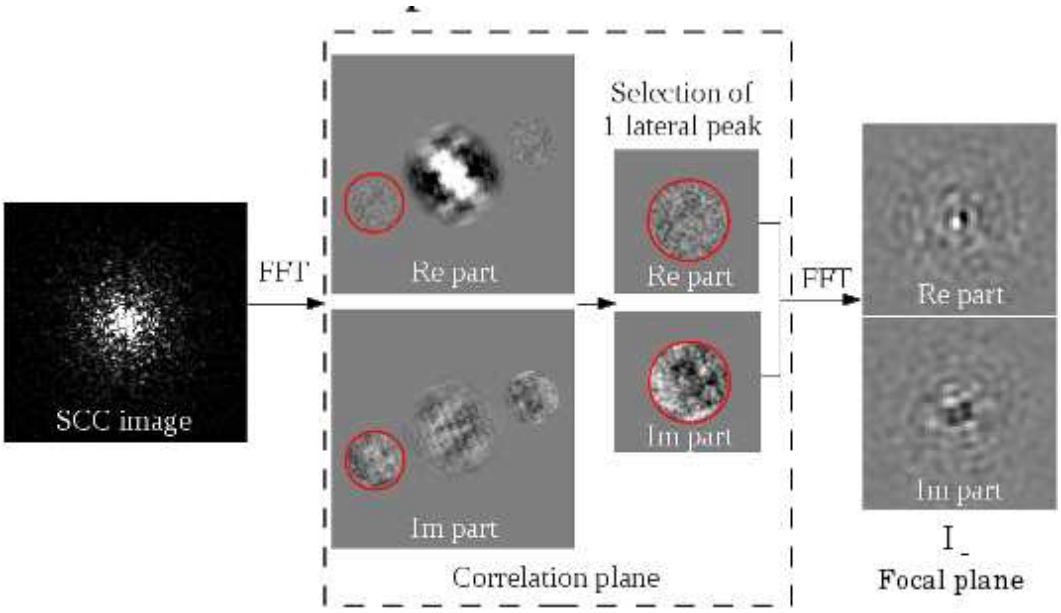


Figure 2. *Estimation of the complex electric field of the speckles.*

reference intensity, and of the planet intensity. The lateral peaks are the correlation between the reference complex field and the speckle complex field.

At this point, one can choose to use the three peaks and combine them to calibrate the speckle intensity in the recorded image a posteriori. This differential imaging mode is presented in previous papers.[21,22,26] An optimization of the algorithm that suppresses the speckles in the image is still to be made but it is outside the scope of the current paper.

If one wants to control a deformable mirror from the science image to create a dark hole, one selects one of the two lateral peaks (they are complex conjugated), and registers it in a new image $FT^{-1}(I_-)$. Taking the Fourier transform of this new image directly leads to $I_-$ which reads

$$I_-(\alpha) = \int_{\mathcal{R}} \frac{1}{\lambda^2} A_{\rm S}\left(\frac{\alpha D}{\lambda}\right) A^*_{\rm R}\left(\frac{\alpha D}{\lambda}\right) \exp\left[2i\pi\alpha\xi_0\left(\frac{1}{\lambda} - \frac{1}{\lambda_0}\right)\right] d\lambda \quad (2)$$

In the monochromatic case, $I_-$ is proportional to $A_{\rm S}\left(\frac{\alpha\, D}{\lambda_0}\right)\, A^*_{\rm R}\left(\frac{\alpha\, D}{\lambda_0}\right)$. In other words, $I_-$ is the multiplication of the complex electric field of the speckles by the complex electric field of the reference channel. One can adjust the size of $FT^{-1}(I_-)$ so that the sampling in $I_-$ is two pixels per resolution element ($\lambda_0/D$).

As explained in our previous papers, the diameter of the reference channel is very small with respect to the diameter of the science beam. So, $A_{R}*$ – very similar to the complex amplitude of an Airy pattern – is almost uniform in the $I_-$ image and $I_-$ is almost proportional to the complex amplitude of the electric field that is associated to the speckles. $I_-$ is thus the estimator that is used to control the deformable mirror in the rest of the paper. Note that the non-uniformity of $A_{R}*$ over the field of view of $I_-$ is not a limitation of the technique as explained in the next section.

### 2.3 Control the deformable mirror

Once one has the estimator of the complex field of the speckles, one needs to find how to control the deformable mirror to create the dark hole in the image. In several techniques, a complete theoretical model of the deformable mirror and of the propagation of the light through the instrument is required for this control. In the case of the self-coherent camera, no theoretial model is needed. To know how the $N \times N$ deformable mirror behaves, we apply $N \times N$ different shapes $S_i$ on the deformable mirror and record for each of them the corresponding estimated electric field $I_{-,i}$. The $N \times N$ $I_{-,i}$ compose the interaction matrix of the instrument and we apply the formalism presented in a previous paper[31] to derive the control matrix of the instrument. As the estimation of the complex electric field of the speckles is done in the focal plane, we choose the $N \times N$ different sinus/cosinus shapes that the deformable mirror can produce. Doing so, the energy is localized in two speckles in each $I_{-,i}$, which increases the signal-to-noise ratio of the measurements.

We note that the control matrix includes the non-uniformity of $A_{R}*$ over the field-of-view. There is thus no need to record or make any assumption on the reference distribution of light in the focal plane of the instrument whereas it was required with the previous estimator .[31]

## 3. EXPERIMENTAL PERFORMANCE

### 3.1 THD-bench

The THD-bench was designed to test under the same conditions several coronagraphs, and active or passive techniques for speckle suppression. It is fully described in a previous paper[28] and we recall the main components that we use in the experiment reported in this paper (Fig. 3).

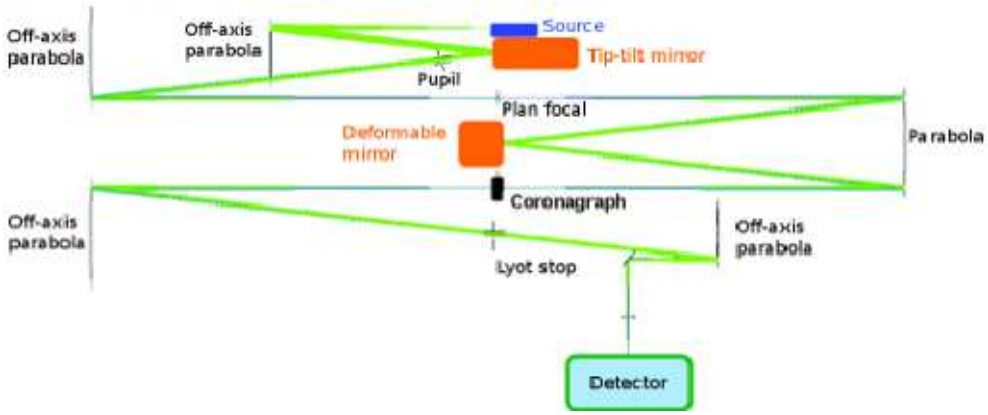


Figure 3. *Layout of the THD-bench.*

The bench is fed by a laser-diode (637 nm) and is composed only by reflective optics creating three pupil planes where we put 1/ a tip-tilt mirror and a 8.1mm unobscurated entrance pupil; 2/ a $32 \times 32$ Boston Micromachines deformable mirror with a pitch of 0.300 mm (27 actuators accross the pupil); 3/ and a Lyot stop of 8 mm (99%

filtering) plus a reference pupil of 0.350 mm with $\xi_0 = 13$ mm. In the focal plane that follows the deformable mirror, we put a monochromatic four quadrant phase mask optimized for 637 nm. The detector is a CMOS camera of $2560 \times 2160$ ($400 \times 400$ used) with a read-out noise of 1.3 e-/pixel and a full well capacity of $\sim 34,000$e-. All the motors, the tip-tilt mirror, the deformable mirror, and the detector are driven via Labview.

### 3.2 Performance in monochromatic light

In this experiment, we use the procedure described in § 2.2 and § 2.3 to control the deformable mirror from the SCC image. The correction converges quickly (10 iterations, i.e. 10 images) and a dark hole is created on the detector (Fig. 4). The $1\,\sigma$-contrast curves of the images before (raw coronagraphic image) and after correction

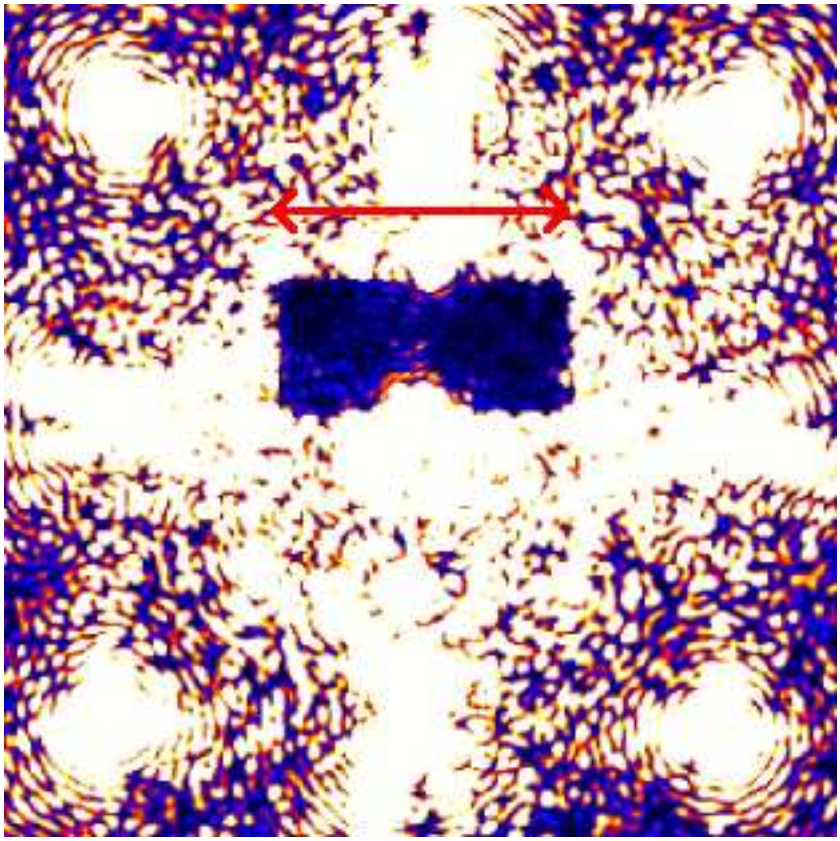

Figure 4. *Experimental image in monochromatic light after correction with one deformable mirror. The arrow length is 27 $\lambda/D$.*

are plotted in Fig. 5. The contrast is the ratio of the root mean square of the intensity calculated in annulii of $1\,\lambda/D$ inside the dark hole and the maximum of the non-coronagraphic image. The contrast after correction reaches $\sim 1.5\,10^{-8}$ between 5 and $12\,\lambda/D$, which corresponds to a gain of 100 in contrast with respect to the image before correction. As demonstrated in a previous publication,[25] the current performance is not limited by the self-coherent camera but by the amplitude errors induced by the deformable mirror. Different solutions are considered to correct for these amplitude aberrations: apodization of the beam after the coronagraph or use of a second deformable mirror or a spatial light modulation.

## 4. ACHROMATIC SCC

### 4.1 Limitation in polychromatic light

In narrow bands ($\lambda/\Delta\lambda \sim 60$) around the coronagraph optimized wavelength $\lambda_c$, we demonstrated in lab that the performance of the correction driven by the SCC is very similar to the monochromatic case and still limited

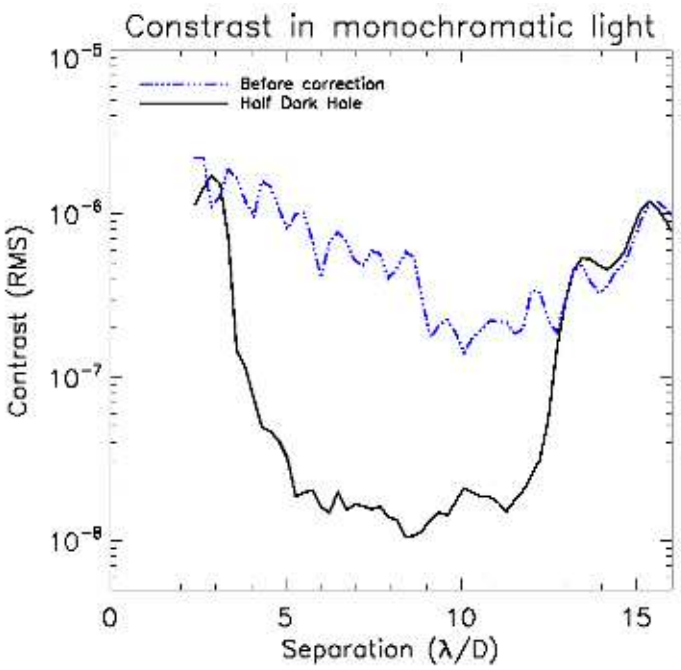


Figure 5. 1 $\sigma$-*contrast curve of the image in the dark hole before (blue mixed curve) and after (black full curve) correction using a SCC.*

by amplitude aberrations.[32] We also found that when the central wavelength of the filter is further than a few tens of nanometers from $\lambda_c$, the image after correction is dominated by the chromatic leak induced by the monochromatic four quadrant phase mask.[32] Thus, it is not possible to test the SCC performance at these wavelengths with the current setup even if there is no reason why it should not work.

Assuming an achromatic coronagraph and a broadband filter ($\lambda/\Delta\lambda \sim 20$), the current version of the self-coherent camera (i.e. with one reference channel) will not be as efficient as it is in monochromatic or quasi-monochromatic light. Indeed, in broadband, the fringes will get blurred going away from the center of the image in one direction (perpendicular to the fringe direction). Where the fringes are blurred, the speckles are not encoded and thus, the aberrations that induce them are not well estimated. That is why in polychromatic light, with a single deformable mirror to correct both phase and amplitude aberrations, only one quarter of the dark hole can be efficiently corrected by the 1-reference-channel SCC described in Fig. 1. As an example, the left image in Fig. 6 is the best correction obtained on the THD-bench using a 1-reference-channel SCC in broadband ($\lambda/\Delta\lambda \sim 18$): only the right top quarter of the dark hole is efficiently corrected. Note that in that image two perpendicular fringe patterns encode the speckles but only one of them is used to control the deformable mirror (see § 4.2).

### 4.2 The two-reference SCC

To improve the performance in polychromatic light, several upgrades of the SCC are proposed. One of the solutions is the two-reference SCC. We showed that the Fizeau fringes are well contrasted in the fringe direction but are blurred in the perpendicular direction. We propose to add a second set of fringes perpendicular to the first Fizeau fringes so that at least one of the two Fizeau patterns spatially modulates any speckle in the field-of-view. To do so, we only add a second reference channel in the Lyot stop at $\sim 90$ degrees from the first reference. A forthcoming paper will fully explain how we retrieve the complex amplitude of the electric field in broadband from the two fringe patterns that spatially modulate the science image.

In § 2.2, we assumed $\xi_0 > 1.5D$. In already designed instrument, the optics after the Lyot stop are not always large enough to obey this assumption. If $\xi_0 < 1.5D$ in the case of a 1-reference SCC, the lateral peaks overlap the

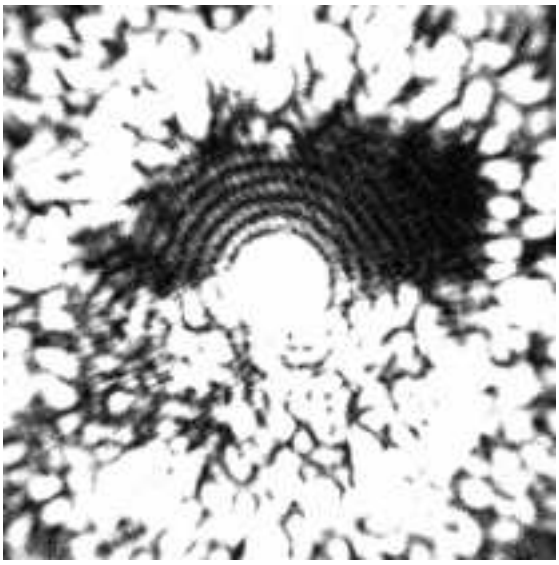

Figure 6. *Experimental dark hole after a 1-reference SCC correction in broadband ($\lambda/\Delta\lambda \sim 20$).*

central peak in the correlation plane (left image in Fig. 7). Thus, part of the information on the encoded speckles is lost, the correction is not efficient, and there is not interest of implementing the SCC to these instruments. If two or three reference channels are used, there are two or three pairs of lateral peaks (right image in Fig. 7). We can combine the information of each pair to retrieve the lost information and obtain an estimation of the electric field in the complete dark hole. A complete study of the multi-reference SCC (behavior in broadband and interest when $\xi_0 < 1.5D$) will be presented in the forthcoming paper.

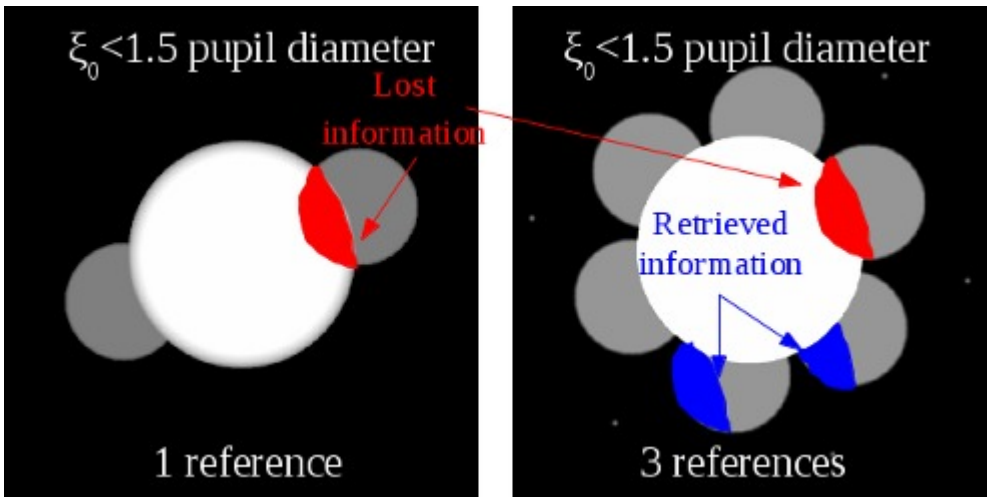


Figure 7. *Fourier transform of the SCC image when one (left) or three (right) reference channels are used.*

### 4.3 Other achromatic SCC

First, we can associate a 1-reference SCC to a Wynne compensator (Fig. 8). The output of the SCC is composed of two polychromatic beams: the reference channel and the science channel. The two triplets of the Wynne compensator change the size of the beams and their separation, the changes being wavelength-dependent. In the output of the SCC-Wynne compensator, the sizes and the separation are proportional to wavelength so that in

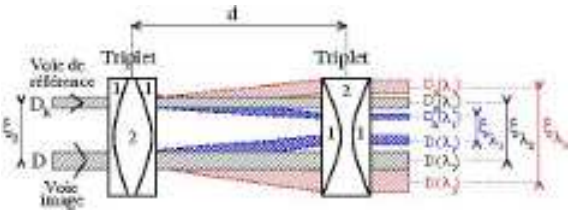


Figure 8. *Association of a SCC and a Wynne compensator.*

the final image, the speckle dispersion ($\lambda/D(\lambda)$) and the fringe period ($\lambda/\xi_0(\lambda)$) are the same for all wavelengths: the fringes are not blurred anymore and the monochromatic procedure for correction (§ 2.2 and § 2.3) is available.

Another solution to achromatize the SCC is the association of the monochromatic version of the SCC with an integral field spectrometer (IFS). In that case, each spectral channel of the IFS provides a quasi-monochromatic image where the speckles are spatially modulated (no blurred fringes in the dark hole). The monochromatic procedure can be used to control the deformable mirror and create a dark hole in the science image. It is important to notice that the SCC will use each spectral channel image independently. In other words, the SCC+IFS instrument will provide an estimation of the complex electric field in the science image as a function of the wavelength with no assumption on the chromatic evolution of the aberrations. A forthcoming paper may study in detail the association of an IFS and a SCC.

## 5. CONCLUSIONS

The current paper is a review of the different works we did on the technique called self-coherent camera (SCC). We do not aim to present all the results that were presented in previous papers[21–32] but to highlight the interesting properties of the techniques.

In § 2, we present the principle of the self-coherent camera (SCC) that spatially modulates the speckles in the science image. We explain that from one single SCC image we can 1/ apply a differential imaging algorithm to enhance the contrast a posteriori and 2/ estimate the complex electric field associated to the speckles and thus, control a deformable mirror to create a dark hole in the science image with no non-common path error.

In § 3, we present experimental results obtained in monochromatic light on the THD-bench and we show the amplitude aberrations induced by the Boston Michromachines deformable mirror are limiting the performance in the current version of the THD-bench. As more results in narrow and large bands are presented in another paper of the same conference,[32] we do not report these results in the current paper.

Finally, in § 4, we study the impact of chromatism on the SCC performance and we propose three ways for the achromatization of the instrument. First, we use two reference channels instead of one (§ 4.2). In that case, the speckles are modulated by two perpendicular Fizeau patterns. Writing the expression of the intensity in the science image, we expect the complex electric field can be estimated in the whole field-of-view controlled by the deformable mirror. We will confirm this result with experimental data taken on the THD-bench in broadband ($\lambda/\Delta\lambda \sim 20$) in a forthcoming paper.

We also propose an association of the SCC with a Wynne compensator or with an integral field spectrometer (§ 4.3). The Wynne compensator spectrally scatters the beams that exits the SCC in order to compensate for the speckle and the fringe spectral dispersion. In other words, the image in polychromatic light is similar to the monochromatic image and the monochromatic estimator can be used with no loss of efficiency for the correction. The association of the SCC with an integral field spectrometer (IFS) seems also interesting but has not been fully studied yet: the SCC will provide an independent estimation of the complex electric field in the science image for each spectral channel of the IFS. Forthcoming papers will study these different setups for an achromatic SCC.

In a near future, we will add an active components on the THD-bench to correct for the amplitude aberrations that currently limit the monochromatic performance in our experiment. We will also replace the monochromatic four quadrant phase mask that we currently use by a more achromatic coronagraph. We will test a multi-stage four quadrant phase mask[10,11] and a dual-zone phase mask.[33]

We will also study the association of the SCC with a vortex coronagraph[8] for IRIS/NFIRAOS for TMT,[34] a space mission that may be proposed to the Canadian Space Agency, another space mission, SPICES,[35] that will be proposed to the next ESA call for proposals for L-missions, and a new high contrast imaging instrument for the Palomar telescope.

## REFERENCES


[1] Lagrange, A., Gratadour, D., Chauvin, G., Fusco, T., Ehrenreich, D., Mouillet, D., Rousset, G., Rouan, D., Allard, F., Gendron, É., Charton, J., Mugnier, L., Rabou, P., Montri, J., and Lacombe, F., "A probable giant planet imaged in the $\beta$ Pictoris disk. VLT/NaCo deep L'-band imaging," *Astronomy & Astrophysics* **493**, L21–L25 (Jan. 2009).

[2] Marois, C., Macintosh, B., Barman, T., Zuckerman, B., Song, I., Patience, J., Lafrenière, D., and Doyon, R., "Direct Imaging of Multiple Planets Orbiting the Star HR 8799," *Science* **322**, 1348– (Nov. 2008).

[3] Roddier, F. and Roddier, C., "Stellar coronograph with phase mask," *Publications of the Astronomical Society of the Pacific* **109**, 815–820 (July 1997).

[4] Aime, C., Soummer, R., and Ferrari, A., "Total coronagraphic extinction of rectangular apertures using linear prolate apodizations," *Astronomy and Astrophysics* **389**, 334–344 (July 2002).

[5] Kuchner, M. J. and Traub, W. A., "A coronagraph with a band-limited mask for finding terrestrial planets," *The Astrophysical Journal* **570**, 900–908 (May 2002).

[6] Kasdin, N. J., Vanderbei, R. J., Littman, M. G., and Spergel, D. N., "Optimal one-dimensional apodizations and shaped pupils for planet finding coronagraphy," *Applied Optics* **44**, 1117–1128 (Mar. 2005).

[7] Guyon, O., Pluzhnik, E. A., Galicher, R., Martinache, F., Ridgway, S. T., and Woodruff, R. A., "Exoplanet imaging with a phase-induced amplitude apodization coronagraph. i. principle," *The Astrophysical Journal* **622**, 744–758 (Mar. 2005).

[8] Mawet, D., Riaud, P., Absil, O., and Surdej, J., "Annular groove phase mask coronagraph," *The Astrophysical Journal* **633**, 1191–1200 (Nov. 2005).

[9] Rouan, D., Riaud, P., Boccaletti, A., Clénet, Y., and Labeyrie, A., "The four-quadrant phase-mask coronagraph. i. principle," *Publications of the Astronomical Society of the Pacific* **112**, 1479–1486 (Nov. 2000).

[10] Baudoz, P., Galicher, R., Baudrand, J., and Boccaletti, A., "Theory and laboratory tests of the multi-stage phase mask coronagraph," in [*Society of Photo-Optical Instrumentation Engineers (SPIE) Conference Series*], *Presented at the Society of Photo-Optical Instrumentation Engineers (SPIE) Conference* **7015** (July 2008).

[11] Galicher, R., Baudoz, P., and Baudrand, J., "Multi-stage four-quadrant phase mask: achromatic coronagraph for space-based and ground-based telescopes," *Astronomy and Astrophysics* **530**, A43+ (June 2011).

[12] Boccaletti, A., Riaud, P., Baudoz, P., Baudrand, J., Reess, J.-M., and Rouan, D., "Coronagraphy with JWST in the thermal IR," in [*EAS Publications Series*], Aime, C. and Soummer, R., eds., *EAS Publications Series* **12**, 195–204 (2004).

[13] Boccaletti, A., Riaud, P., Baudoz, P., Baudrand, J., Rouan, D., Gratadour, D., Lacombe, F., and Lagrange, A.-M., "The four-quadrant phase mask coronagraph. iv. first light at the very large telescope," *Publications of the Astronomical Society of the Pacific* **116**, 1061–1071 (Nov. 2004).

[14] Mawet, D., Absil, O., Delacroix, C., Girard, J. H., Milli, J., O'Neal, J., Baudoz, P., Boccaletti, A., Bourget, P., Christiaens, V., Forsberg, P., Gonte, F., Habraken, S., Hanot, C., Karlsson, M., Kasper, M., Lizon, J.-L., Muzic, K., Olivier, R., Peña, E., Slusarenko, N., Tacconi-Garman, L. E., and Surdej, J., "L'-band AGPM vector vortex coronagraph's first light on VLT/NACO. Discovery of a late-type companion at two beamwidths from an F0V star," *Astronomy & Astrophysics* **552**, L13 (Apr. 2013).

[15] Marois, C., Lafrenière, D., Doyon, R., Macintosh, B., and Nadeau, D., "Angular Differential Imaging: A Powerful High-Contrast Imaging Technique," *The Astrophysical Journal* **641**, 556–564 (Apr. 2006).

[16] Marois, C., Racine, R., Doyon, R., Lafrenière, D., and Nadeau, D., "Differential imaging with a multicolor detector assembly: A new exoplanet finder concept," *The Astrophysical Journal Letter* **615**, L61–L64 (Nov. 2004).

[17] Baba, N. and Murakami, N., "A method to image extrasolar planets with polarized light," *Publications of the Astronomical Society of the Pacific* **115**, 1363–1366 (Dec. 2003).

[18] Bordé, P. J. and Traub, W. A., "High-contrast imaging from space: Speckle nulling in a low-aberration regime," *Astrophysical Journal* **638**, 488–498 (Feb. 2006).

[19] Give'on, A., Kern, B., Shaklan, S., Moody, D. C., and Pueyo, L., "Electric Field Conjugation - A Broadband Wavefront Correction Algorithm For High-contrast Imaging Systems," in [*American Astronomical Society Meeting Abstracts*], *Bulletin of the American Astronomical Society* **39**, 135.20 (Dec. 2007).

[20] Pueyo, L., Shaklan, S., Give'On, A., and Krist, J., "Numerical propagator through PIAA optics," in [*Society of Photo-Optical Instrumentation Engineers (SPIE) Conference Series*], *Society of Photo-Optical Instrumentation Engineers (SPIE) Conference Series* **7440** (Aug. 2009).

[21] Baudoz, P., Boccaletti, A., Baudrand, J., and Rouan, D., "The self-coherent camera: a new tool for planet detection," in [*IAU Colloq. 200: Direct Imaging of Exoplanets: Science Techniques*], Aime, C. and Vakili, F., eds., 553–558 (2006).

[22] Galicher, R. and Baudoz, P., "Expected performance of a self-coherent camera," *Comptes Rendus Physique* **8**, 333–339 (Apr. 2007).

[23] Baudoz, P., Mas, M., Galicher, R., and Rousset, G., "The Self-Coherent Camera : a focal plane sensor for EPICS ?," in [*Adaptative Optics for Extremely Large Telescopes*], (2010).

[24] Baudoz, P., Mas, M., Galicher, R., and Rousset, G., "Focal plane wavefront sensor sensitivity for ELT planet finder," in [*Society of Photo-Optical Instrumentation Engineers (SPIE) Conference Series*], *Society of Photo-Optical Instrumentation Engineers (SPIE) Conference Series* **7736** (July 2010).

[25] Baudoz, P., Mazoyer, J., Mas, M., Galicher, R., and Rousset, G., "Dark hole and planet detection: laboratory results using the self-coherent camera," in [*Society of Photo-Optical Instrumentation Engineers (SPIE) Conference Series*], *Society of Photo-Optical Instrumentation Engineers (SPIE) Conference Series* **8446** (Sept. 2012).

[26] Galicher, R., Baudoz, P., and Rousset, G., "Wavefront error correction and earth-like planet detection by a self-coherent camera in space," *Astronomy and Astrophysics* **488**, L9–L12 (Sept. 2008).

[27] Galicher, R., Baudoz, P., Rousset, G., Totems, J., and Mas, M., "Self-coherent camera as a focal plane wavefront sensor: simulations," *Astronomy and Astrophysics* **509**, A31+ (Jan. 2010).

[28] Mas, M., Baudoz, P., Rousset, G., Galicher, R., and Baudrand, J., "Self-coherent camera: first results of a high-contrast imaging bench in visible light," in [*Society of Photo-Optical Instrumentation Engineers (SPIE) Conference Series*], *Society of Photo-Optical Instrumentation Engineers (SPIE) Conference Series* **7735** (July 2010).

[29] Mas, M., Baudoz, P., Mazoyer, J., Galicher, R., and Rousset, G., "Experimental results on wavefront correction using the self-coherent camera," in [*Society of Photo-Optical Instrumentation Engineers (SPIE) Conference Series*], *Society of Photo-Optical Instrumentation Engineers (SPIE) Conference Series* **8446** (Sept. 2012).

[30] Mazoyer, J., Baudoz, P., Mas, M., Rousset, G., and Galicher, R., "Experimental parametric study of the self-coherent camera," in [*Society of Photo-Optical Instrumentation Engineers (SPIE) Conference Series*], *Society of Photo-Optical Instrumentation Engineers (SPIE) Conference Series* **8442** (Sept. 2012).

[31] Mazoyer, J., Baudoz, P., Galicher, R., Mas, M., and Rousset, G., "Estimation and correction of wavefront aberrations using the self-coherent camera: laboratory results," *Astronomy & Astrophysics* **557**, A9 (Sept. 2013).

[32] Mazoyer, J., Baudoz, P., Galicher, R., and Rousset, G., "Speckle correction in polychromatic light with the Self Coherent Camera Experimental Results," in [*Society of Photo-Optical Instrumentation Engineers (SPIE) Conference Series*], *Society of Photo-Optical Instrumentation Engineers (SPIE) Conference Series* **8864** (2013).

[33] Soummer, R., Dohlen, K., and Aime, C., "Achromatic dual-zone phase mask stellar coronagraph," *Astronomy and Astrophysics* **403**, 369–381 (May 2003).

[34] Herriot, G., Andersen, D., Atwood, J., Byrnes, P., Boucher, M.-A., Boyer, C., Caputa, K., Correia, C., Dunn, J., Ellerbroek, B., Fitzsimmons, J., Gilles, L., Hickson, P., Hill, A., Kerley, D., Pazder, J., Reshetov, V., Roberts, S., Smith, M., Véran, J.-P., Wang, L., and Wevers, I., "TMT NFIRAOS: adaptive optics system for the Thirty Meter Telescope," in [*Society of Photo-Optical Instrumentation Engineers (SPIE) Conference Series*], *Society of Photo-Optical Instrumentation Engineers (SPIE) Conference Series* **8447** (July 2012).

[35] Boccaletti, A., Schneider, J., Traub, W., Lagage, P.-O., Stam, D., Gratton, R., Trauger, J., Cahoy, K., Snik, F., Baudoz, P., Galicher, R., Reess, J.-M., Mawet, D., Augereau, J.-C., Patience, J., Kuchner, M., Wyatt, M., Pantin, E., Maire, A.-L., Vérinaud, C., Ronayette, S., Dubreuil, D., Min, M., Rodenhuis, M., Mesa, D., Belikov, R., Guyon, O., Tamura, M., Murakami, N., and Beerer, I. M., "SPICES: spectro-polarimetric imaging and characterization of exoplanetary systems. From planetary disks to nearby Super Earths," *Experimental Astronomy* **34**, 355–384 (Oct. 2012).